Multiobjective Path Placement Optimization of Parallel Kinematics Machines Based on Energy Consumption, Shaking Forces and Maximum Actuators Torques: Application to the Orthoglide

Raza Ur-Rehman, Stéphane Caro, Damien Chablat, Philippe Wenger

Multiobjective Path Placement Optimization of Parallel Kinematics Machines Based on Energy Consumption, Shaking Forces and Maximum Actuators Torques: Application to the Orthoglide

Raza UR-REHMAN, Stéphane CARO

Damien CHABLAT, Philippe WENGER

Institut de Recherche en Communications et Cybernétique de Nantes

UMR CNRS n° 6597, 1 rue de la Noë, 44321 Nantes, France

Tel: +33 2 40 37 69 68, Fax: +33 2 40 37 69 30

{ur-rehman, caro, chablat, wenger}@irccyn.ec-nantes.fr

Abstract

This paper deals with the multi-objective path placement optimization for Parallel Kinematics Machines (PKMs) based on energy consumption, actuators torques and shaking forces. It aims at determining the optimal location of a given test path within the workspace of a PKM in order to minimize the electric energy used by the actuators, their maximal torque and the shaking forces subject to the kinematic, dynamic and geometric constraints. The proposed methodology is applied to the Orthoglide, a three-degree-of-freedom translational PKM, as an illustrative example.

Keywords: Multiobjective Optimization; Path Planning; Parallel Kinematics Machine

1 Introduction

Optimal trajectory planning has been a relevant area for roboticists for many years. Several authors have worked on trajectory planning based on different optimization objectives. A review of trajectory planning techniques is given in [1]. Trajectory planning usually aims at minimizing the travel distance [2], travel or machining time [3, 4] and/or the energy consumed [5, 6], while satisfying several geometric, kinematic and dynamic constraints. The trajectory planning deals with the determination of the path and velocity/acceleration profiles (or the time history of the robot's joints), the start and end points of the trajectory being predefined and fixed in the workspace.

Another less explored aspect of trajectory planning is the placement of a given path within the workspace. It aims at determining the optimum location of a predefined path to be followed by the end-effector of a Parallel Kinematics Machine (PKM) or a robot, within its workspace with respect to one or many given objective(s) and constraint(s). This path can be the shape of a component to be machined, a welded profile or an artistic/decorative profile etc. In such situations, the trajectory planner cannot alter the shape of the path but he/she can only play with the location of that path within the workspace in order to optimize one or several criterion(a). Such an approach can be very interesting in many robotic applications. For example, in machining applications, the location of the workpiece within the workspace may affect the electric energy used by its actuators.

The path placement problem has not been extensively studied in the past. Nevertheless, some researchers proposed to solve it with respect to various optimization objectives. Several performance criteria for path location problems can be considered simultaneously (multiobjective) or individually, such as travel time, different kinetostatic performance indices (such as, manipulability or the conditioning number of the normalized kinematic Jacobian matrix), kinematic performance (velocity, acceleration), collisions, wear and vibration reduction, energy consumption etc.

Nelson and Donath [7] proposed an algorithm for the optimum location of an assembly task

in a manipulator workspace while taking the manipulability measure as the optimization criterion. The location of the assembly task that results in the highest manipulability is considered as optimal position. Aspragathos [8, 9] used the concept of the orientation of the manipulability ellipsoid relative to the desired path and introduced a criterion to characterize the best velocity performance of the robot end-effector with the path location. Fardanesh et al. [10] proposed an approach for optimal positioning of a prescribed task in the workspace of a $2R$-robot arm to minimize the cycle time. In another study, Feddema [11] formulated and solved a problem of robot base placement for a minimum joint motion time within a work cell. The proposed algorithm considers only the kinematics and the maximum acceleration of each joint in order to obtain a 25% cycle time improvement for a typical example. Hemmerle [12] presented an algorithm for optimum path placement of a redundant manipulator by defining a cost function related to robot joints motion and limits. The proposed approach did not consider the path as a whole but discrete points of that path. Pamanes and Zeghloul [13] considered several kinematic indices to find the optimal placement of a robot by specifying the path with a number of points and then assigning an optimization criterion to each point. The objective was to find the path location in order to have optimal values of all the criteria assigned to the path points. In [14], the problem of optimal placement with joint-limits and obstacle avoidance is addressed. Lately, a general formulation was presented to determine the optimal location of a path for a redundant robotic manipulator while dealing with mono- and multi-objective problems [15].

In another relevant work, Wang et al. [16] proposed a mathematical model to determine the right position and orientation of a workpiece in the workspace of a Stewart platform based NC-miller machine tool. The idea of their study was to analyze the effects of geometric and non-geometric constraints on the workspace and subsequently, using these information to determine the right pose of the workpiece in the workspace a parallel machine tool. However, the only objective that they considered was the location of the workpiece for the accessibility of a specific machine tool.

With a general literature survey, it comes out that although several performance indices are

introduced or considered, there is no emphasis on the dynamic aspects reflecting the energy consumption by the PKM actuators, while executing a specific task. Another less explored but important criterion of optimal path placement can be the minimization of the shaking forces and moments experienced by the base of the PKM. Shaking forces and moments can affect the performance of a PKM in terms of excessive loads, accuracy, wear, fatigue, etc. Accordingly, we introduce two indices characterizing the variations and the maximum value of the shaking forces. The maximum actuators torque is considered as another optimization objective. Keeping in view these aspects, the authors recently presented an approach for the optimal path placement for a manipulator based on energy consumption [17]. In the same vein, it is pertinent to follow a multiobjective approach to optimize the location of a path to be followed by the end-effector of a PKM within its workspace. The objectives are to minimize the energy consumed by its actuators, minimize the shaking forces and/or moments and minimize the maximum actuators torques. Finally, the proposed approach is applied to the Orthoglide: a three-degree-of-freedom translational PKM.

The paper is organized as follows: in section 2, a multi-objective path placement optimization problem is formulated, by means of the design variables, the objective functions and the constraints. Moreover, an algorithm is proposed to solve such a problem. In section 3, the optimum locations of a test path within the workspace of the Orthoglide are highlighted.

2 Path Placement Optimization

The problem aims at determining the optimal location of a predefined path to optimize some objective functions. The entire path is supposed to be known within the framework of this research work. The path location can be defined in a similar way as to define the location of a workpiece with respect to a PKM reference point. The optimization problem is composed of three sets, namely, the set of design variables, the set of objective functions and the set of design constraints. Accordingly, the optimization problem aims at determining the design variables, characterizing the path location, in order to minimize the objective functions subject

to the design constraints.

2.1 Decision Variables: Path Location Parameters

In order to formulate and describe the problem, two frames are defined: *i*) the path frame $\mathcal{F}_p$ and *ii*) the base frame $\mathcal{F}_b$, as shown in Fig. 1(a). The path frame $\mathcal{F}_p$, is attached to the given/required path at a suitable point such as the geometric center of the path. As $\mathcal{F}_p$ is attached to the path, the end-effector trajectory parameters remain constant in this reference frame, no matter where it is located, i.e., the path is fully defined and constant in $\mathcal{F}_p$. It can also be named as workpiece frame since it characterizes the position and the orientation of the workpiece within the workspace. The base frame $\mathcal{F}_b$ can also be called global or PKM frame. It is attached to the PKM base and is used to locate a workpiece (or $\mathcal{F}_p$) with respect to the PKM coordinate system. The location and orientation of $\mathcal{F}_p$ with respect to $\mathcal{F}_b$ can be defined in such a way that the whole path lies within the workspace. The position of $\mathcal{F}_p$

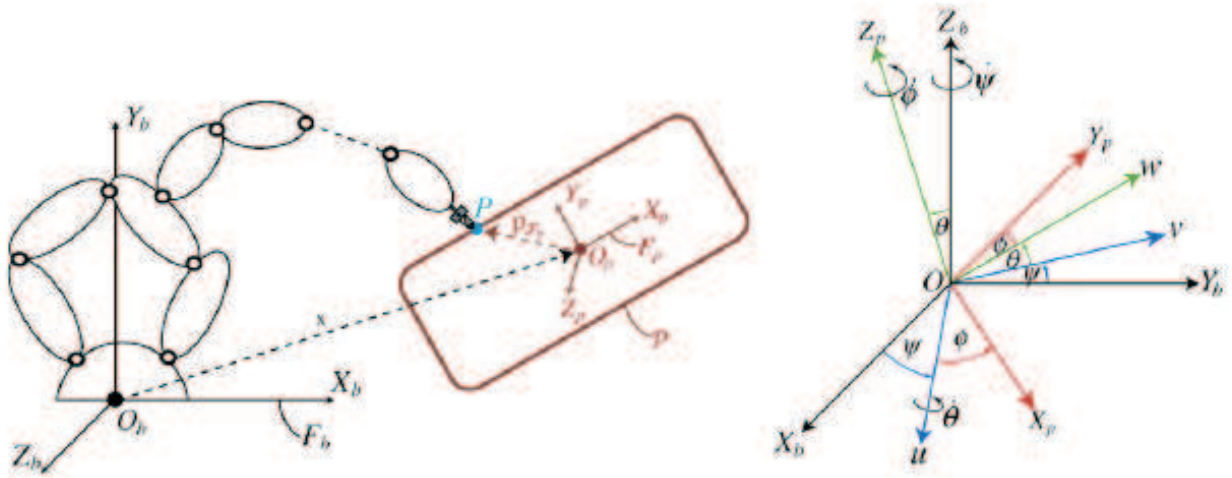

Figure 1: Path placement characterization, $\mathcal{F}_b$ and $\mathcal{F}_p$ being the base and path frames

with respect to $\mathcal{F}_b$ is defined with the Cartesian coordinates of the origin of $\mathcal{F}_p$. The relative orientation of the two frames is characterized by the Euler angles. Accordingly, any trajectory defined in $\mathcal{F}_p$ can be expressed in $\mathcal{F}_b$ by means of a transformation matrix. For instance, the

Cartesian coordinates x_{P_b}, y_{P_b}, z_{P_b} of point P in $\mathcal{F}_b$ are obtained from its Cartesian coordinates x_{P_p}, y_{P_p}, z_{P_p} expressed in $\mathcal{F}_p$ by means of the transformation matrix ${}^b\mathbf{T}_p$ from $\mathcal{F}_p$ to $\mathcal{F}_b$:

$$\begin{bmatrix} x_{P_b} & y_{P_b} & z_{P_b} & 1 \end{bmatrix}^T_{\mathcal{F}_b} = {}^b\mathbf{T}p \begin{bmatrix} x_{P_p} & y_{P_p} & z_{P_p} & 1 \end{bmatrix}^T_{\mathcal{F}_p} \tag{1}$$

Let O_p be the origin of the path frame of Cartesian coordinates $(x_{O_p}, y_{O_p}, z_{O_p})$ expressed in $\mathcal{F}_b$ and let the Euler angles ϕ, θ, ψ characterize the orientation of $\mathcal{F}_p$ with respect to $\mathcal{F}_b$, as shown in Fig. 1(b). The transformation matrix ${}^b\mathbf{T}p$ is expressed as,

$${}^b\mathbf{T}p = \begin{bmatrix} \cos\phi\cos\theta & \cos\phi\sin\theta\sin\psi - \sin\phi\cos\psi & \cos\phi\sin\theta\cos\psi + \sin\phi\sin\psi & x_{O_p} \\ \sin\phi\cos\theta & \sin\phi\sin\theta\sin\psi + \cos\phi\cos\psi & \sin\phi\sin\theta\cos\psi - \cos\phi\sin\psi & y_{O_p} \\ -\sin\theta & \cos\theta\sin\psi & \cos\theta\cos\psi & z_{O_p} \\ 0 & 0 & 0 & 1 \end{bmatrix} \tag{2}$$

Let $\mathbf{x} = [x_{O_p} \quad y_{O_p} \quad z_{O_p} \quad \phi \quad \theta \quad \psi]^T$ define the path location within the workspace in $\mathcal{F}_b$. Then, the components of $\mathbf{x}$ are the decision variables of the optimization problem.

In the context of a general machining process like milling operation, the feature to be machined in the workpiece is defined with respect to its frame, namely $\mathcal{F}_p$. Likewise, the machining operation conditions such as machining velocity and acceleration are fully defined in $\mathcal{F}_p$. Finally the part location in the workspace is defined in $\mathcal{F}_b$.

2.2 Optimization Objectives

The path placement optimization is performed with the aim of minimizing four objective functions, namely, (i) electric energy consumption, (ii) variations in the shaking forces, (iii) maximum shaking forces and (iv) maximum actuators torques. In the following sections, the mathematical expressions of these objective functions are given.

2.2.1 Electric Energy

The energy used by the motors depends on their velocity and torque. As the electric current drawn varies with motors required velocities and torques, the motor's self-inductance phenomenon appears. The current I drawn by the motors and the motor electromotive potential V_e can be calculated as a function of the required torque τ and the angular velocity ω of the actuators, namely,

$$I = \tau / K_t \tag{3}$$

$$V_e = K_e \omega \tag{4}$$

K_t being the torque sensitivity factor expressed in [Nm/A] and K_e the back electromotive force constant expressed in [V.(rad/sec)$^{-1}$]. The total electric power P_T is composed of resistive power loss, P_J; inductive power loss, P_L; and the power used to produce electromotive force, P_{EM} [18], i.e.,

$$P_T = P_J + P_L + P_{EM} \tag{5}$$

where

$$P_J = RI^2 \quad , \quad P_L = LI\frac{dI}{dt} \quad , \quad P_{EM} = V_e I \tag{6}$$

R being the motor winding resistance expressed in Ohm [Ω] and L the motor inductance coefficient expressed in Henry [H]. Finally, the energy E consumed by a motor can be evaluated by integrating P_T over the total trajectory time T, namely,

$$E = \int_0^T P_T dt \tag{7}$$

P_T being the instantaneous electric power at instantaneous time t, defined in Eq. (5).

It should be noted that Eq. (3) allows us to consider the energy used by the actuators while they do not move but still produce a torque to keep the PKM at a certain stationary configuration (with respect to that particular direction or actuator). Finally, the total energy E_t consumed by n actuators can be written as:

$$E_t = \sum_{i=1}^{n} E_i \tag{8}$$

E_i being the total electric energy required by the i^{th} actuator, given by Eq. (7). Consequently, the first objective of the path placement optimization problem can be written as:

$$f_1(\mathbf{x}) = E_t \rightarrow \min \tag{9}$$

2.2.2 Shaking Forces

Shaking or dynamic forces and moments are the inertial forces and moments exerted on the base of a PKM due to the uneven mass distribution. These forces/moments may deteriorate system performance by introducing excessive vibration, noise, wear and fatigue. Furthermore required input torques and forces may also increase to account for these shaking effects. Hence, in order to overcome these drawbacks and to improve system performance in terms of accuracy, precision, fatigue life, vibration reduction, motion planning and control, the study of the shaking forces and moments is of prime importance.

Dynamic balancing has been an area of research for some decades and several authors have contributed to this domain by formulating and analyzing the problems for either some particular applications or for more general prospects [19, 20, 21]. Here, we will use this concept in order to optimize the path location within the workspace of the PKM to minimize the shaking forces effects.

For the purpose of simplicity, shaking forces are exclusively considered in this research work while shaking moments are left for future works.

In order to assess the effect of shaking forces, two indices are proposed, namely,

1. Shaking force variation index, $I_{\delta f}$, considers the maximum variation in the shaking forces along the trajectory, i.e.,

$$I_{\delta f} = \max\ (dF_{sh}) \tag{10}$$

where $dF_{sh} = \sum_{i=1}^{n} dF_{sh}^i$ is the sum of the variations in the n shaking forces, n being the number of limbs. The variation in the shaking forces for the i^{th} limb is given by,

$$dF_{sh}^i = \sqrt{\left[\max(\mathbf{F}_x^i) - \min(\mathbf{F}_x^i)\right]^2 + \left[\max(\mathbf{F}_y^i) - \min(\mathbf{F}_y^i)\right]^2 + \left[\max(\mathbf{F}_z^i) - \min(\mathbf{F}_z^i)\right]^2} \tag{11}$$

where $\mathbf{F}_x^i, \mathbf{F}_y^i$ and $\mathbf{F}_z^i$ are $1 \times N_t$ dimensional vectors, representing the respective force profile along trajectory, N_t being the number of time steps. The variations in the shaking forces will influence the base platform vibrations. Hence, the second objective function of the path optimization problem can be written as,

$$f_2(\mathbf{x}) = I_{\delta f} \rightarrow \min \tag{12}$$

2. Maximum shaking force index, I_f, characterizes the magnitude of the maximum shaking forces experienced by the base platform along the trajectory, i.e.,

$$I_f = \max\ (\mathbf{F}_{sh}) \tag{13}$$

where $\mathbf{F}_{sh} = \sum_{i=1}^{n} \mathbf{F}_{sh}^i$ is $1 \times N_t$ dimensional vector representing the sum of the shaking forces experienced by the n limbs with N_t time steps. The maximum shaking force gives an idea of the maximum extra loads experienced by the actuators resulting from the shaking forces, for a particular trajectory. Hence the knowledge of the maximum shaking forces can help the designer to select the appropriate actuators to cater for these excessive loads on the system. Accordingly, the third objective function of the path optimization problem can be written as,

$$f_3(\mathbf{x}) = I_f \rightarrow \min \tag{14}$$

2.2.3 Maximum Torque

In order to reduce the actuators loads, the magnitude of the maximum torque τ_{max} experienced by the PKM actuators is considered. For a PKM of n actuators, τ_{max} is defined as,

$$\tau_{max} = \max(\tau_{1_{max}}, \ldots, \tau_{i_{max}}, \ldots, \tau_{n_{max}}) \tag{15}$$

$\tau_{i_{max}}$ being the magnitude of the maximum torque experienced by the i^{th} actuator along the trajectory. Consequently, the fourth objective function of the path optimization problem can be written as,

$$f_4(\mathbf{x}) = \tau_{max} \rightarrow \min \tag{16}$$

2.3 Constraints

The path placement optimization problem is subject to geometric, kinematic and dynamic constraints. Geometric constraints include joint limits and the boundaries of the workspace. Kinematic constraints deal with the maximum actuators velocities whereas dynamic constraints are related to actuators wrenches, namely,

$$q_{il} \leq q_i \leq q_{iu} \quad , \quad \dot{q}_i \leq \dot{q}_{iu} \quad , \quad \tau_i \leq \tau_{iu} \tag{17}$$

q_i, $\dot{q}_i$, τ_i are respectively the i^{th} actuator displacement, rate and torque. q_{il} is the lower bound and q_{iu} (resp. $\dot{q}_{iu}$ and τ_{iu}) is the upper bound of i^{th} actuator displacement (resp. rate and torque). For a given path placement vector $\mathbf{x}$, these constraints can be evaluated by means of the PKM kinematic, velocity and dynamic models.

It is noteworthy that the PKM geometric constraints guarantee that the whole path lies inside the prescribed workspace. Similarly, the bounds on actuators rate ($\dot{q}_{iu}$) and torque (τ_{iu}) ensure that the PKM will not go through any singular configuration while following the path.

2.4 Problem Statement and Solution

The goal of this research work is to help the path planner find the best location of the path to be followed by the PKM in order to minimize the four objective functions defined in the foregoing subsections. The multi-objective path placement optimization problem can be formulated as:

"*For a predefined path in $\mathcal{F}_p$, find the optimum location and orientation of $\mathcal{F}_p$ with respect to $\mathcal{F}_b$, defined by the decision variables* $\mathbf{x}$*, in order to minimize the objective functions f_1, f_2, f_3 and f_4 while respecting the kinematic, velocity and dynamic constraints of the PKM*"

Mathematically, the problem can be formulated as follows:

$$\min_{\mathbf{x}} \left(f_1(\mathbf{x}),\ f_2(\mathbf{x}),\ f_3(\mathbf{x}),\ f_4(\mathbf{x})\right) \qquad \text{subject to:} \begin{cases} q_{il} \leq q_i \leq q_{iu} \\ \dot{q}_i \leq \dot{q}_{iu} \\ \tau_i \leq \tau_{iu} \end{cases} \tag{18}$$

To solve the problem, a general optimization approach based on Multi-Objective Genetic Algorithm (MOGA) is proposed as illustrated in Fig. 2. Starting with the input variables, the inverse kinematic model (IKM), the inverse velocity model (IVM) and the inverse dynamic model (IDM) of the PKM are used to determine the objectives functions and constraints for particular designs variables. MOGA is used to generate the initial population, evaluate the objective functions and constraints in order to generate new populations by carrying out the reproduction, cross over and mutation operations. The Pareto optimal solutions are obtained from the final feasible population.

3 Case Study: Application to the Orthoglide

3.1 Description of the Orthoglide

The Orthoglide is a Delta-type PKM [22] dedicated to 3-axis rapid machining applications developed in IRCCyN [23]. It gathers the advantages of both serial and parallel kinematic architectures such as regular workspace, homogeneous performances, good dynamic performances and stiffness. The Orthoglide is composed of three identical legs, as shown in Fig. 3(a). Each leg is made up of a prismatic joint, two revolute joints and a parallelogram joint. Only the prismatic joints of the legs are actuated.

The Orthoglide geometric parameters are function of the size of the prescribed Cartesian

Table 1: Orthoglide workspace parameters

Workspace size $L_{workspace} = 0.2$ m	
Point	Cartesian coordinates in $\mathcal{F}_b$ [m]
O_b	$(0, 0, 0)$
C	$(-0.027, -0.027, -0.027)$
Q^+	$(0.73, 0.73, 0.73)$
Q^-	$(-0.127, -0.127, -0.127)$

workspace, namely, $L_{workspace}$ [24]. The base frame $\mathcal{F}_b$ is defined with the prismatic actuators axes, namely, X_b, Y_b and Z_b, the origin O_b of $\mathcal{F}_b$ being their common intersection point. Two

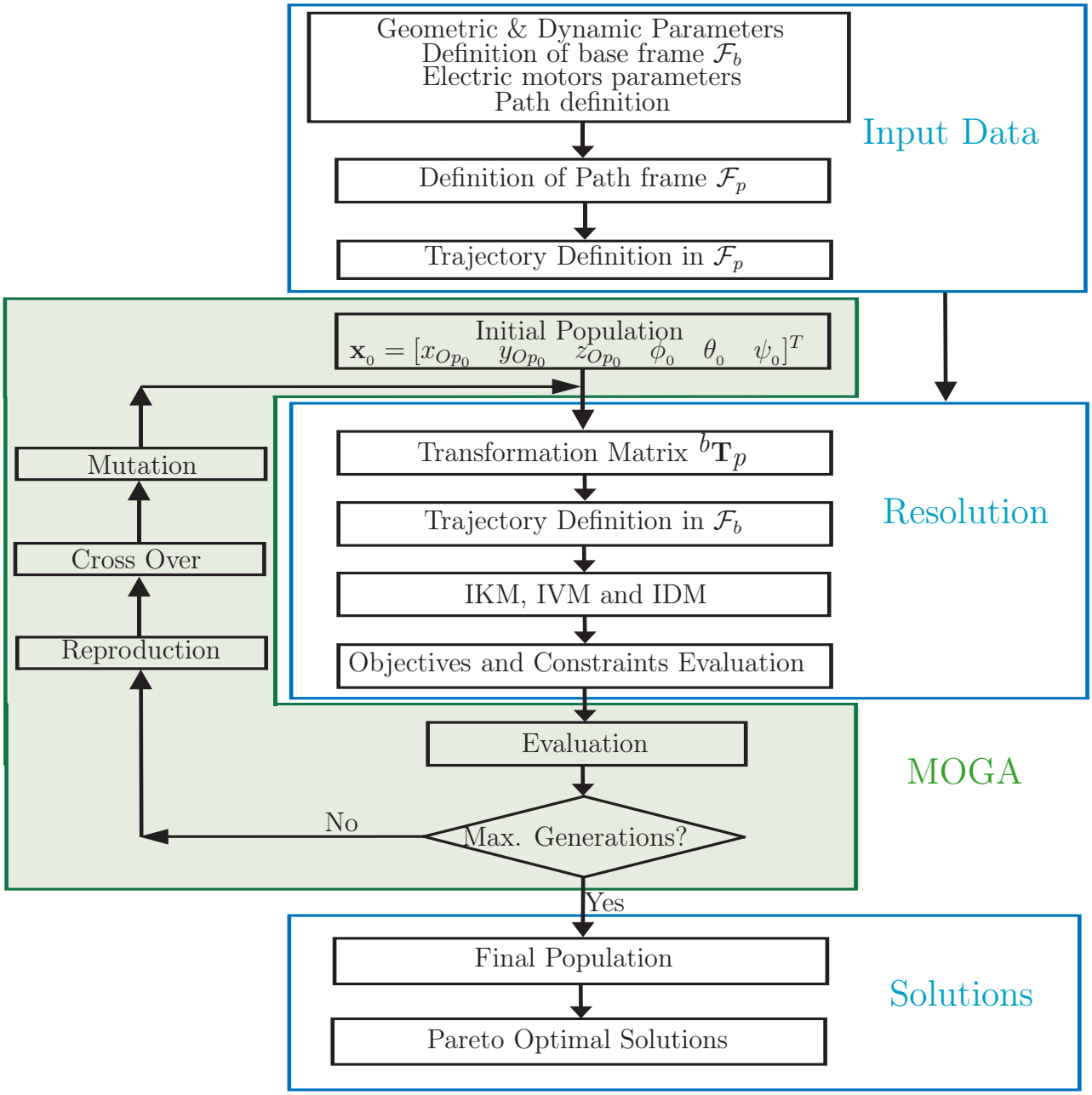

Figure 2: Flowchart of the path location optimization process

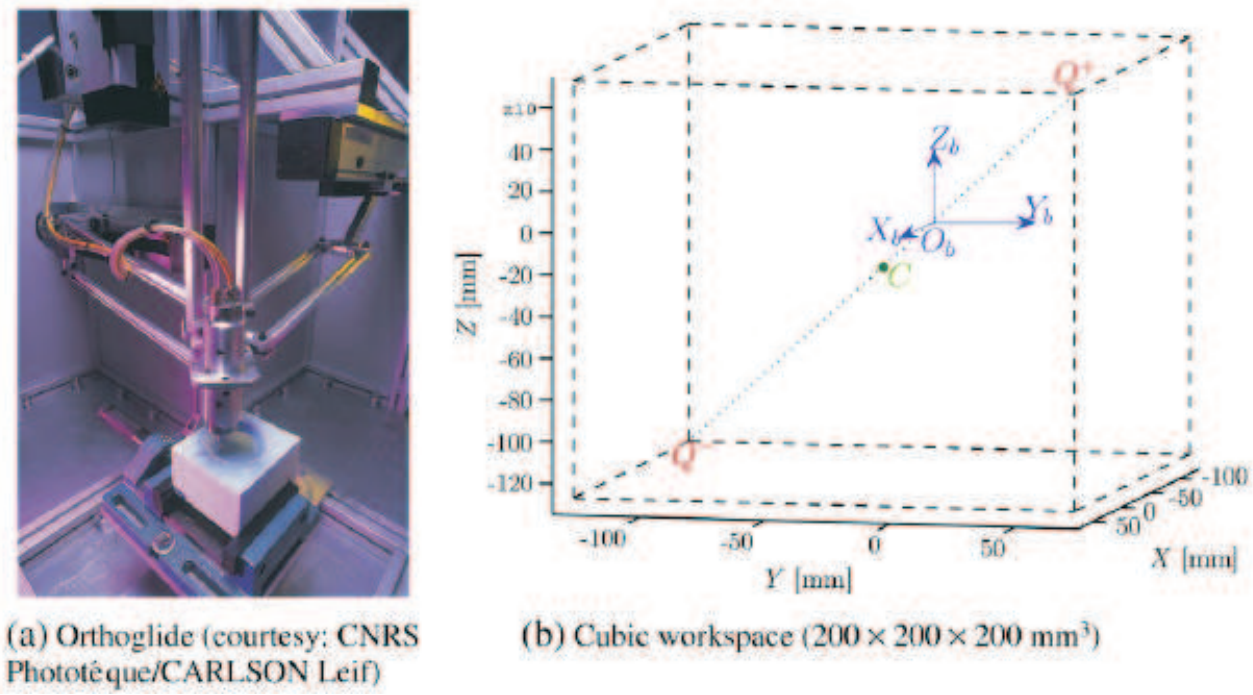

(a) Orthoglide (courtesy: CNRS Photothèque/CARLSON Leif)

(b) Cubic workspace ($200 \times 200 \times 200$ mm^3)

Figure 3: A snap and workspace of the Orthoglide

points Q^+ and Q^- are defined in such a way that the transmission factor is 1/2 and 2 at these two points [25]. A cube is then constructed with Q^+Q^- as its diagonal. It should be noted that the cubic workspace center, i.e., point C, and the origin O_b of the reference frame $\mathcal{F}_b$ do not coincide, as shown in Fig. 3(b). In the scope of this study, $L_{workspace}$ is equal to 0.200m. Accordingly, the coordinates of points Q^+, Q^- and C for the said workspace are given in Table 1. Similarly, the prismatic actuators bounds, ρ_{min} and ρ_{max}, can be calculated [24]. Table 2 shows the lower and upper bounds of the prismatic joints displacements and their maximum allowable velocity and torque for the Orthoglide. The geometric, kinematic and dynamic parameters of the Orthoglide are defined in [23, 24, 25, 26].

Table 2: Orthoglide actuators parameters ($i = x, y, z$)

$\rho_{i_{min}}$	0.126 m
$\rho_{i_{max}}$	0.383 m
$v_{i_{max}}$	1.00 m.s^{-1}
$\tau_{i_{max}}$	1.274 Nm

3.2 Objective Functions Formulation for the Orthoglide

3.2.1 Electric Energy for the Orthoglide

The electric energy E_i used by each actuator is calculated by means of Eqs. (3)-(7). As the Orthoglide has three *3-phase Sanyo Denki* synchronous servo motors ($reference : P30B0604D$), Eq. (5) is multiplied by 3 to cater for the power consumed by the each phase of the motor in order to calculate the electric power P_{Ti} used by each actuator, i.e.,

$$P_{T_i} = 3(RI^2 + LI\frac{dI}{dt} + V_e I) \tag{19}$$

3.2.2 Shaking forces formulation for the Orthoglide

Shaking forces $\mathbf{f}_{sh}$ at the base platform of a PKM depend on the mass and the acceleration of the center of mass of each moving element. For a system of w masses, $\mathbf{f}_{sh}$ can be expressed as:

$$\mathbf{f}_{sh} = \sum_{j=1}^{w} m_j \ddot{c}_j \tag{20}$$

where m_j is the mass and $\ddot{c}_j$ is the acceleration of the center of mass of the j^{th} element. In order to calculate the shaking forces at the Orthoglide base-frame, three reference frames, corresponding to each leg, are defined at points A_1, A_2 and A_3, as shown in Fig. 4. The shaking forces for each leg are calculated independently in the respective reference frame. Each leg is supposed to be composed of six components, namely,

M_1: foot of length L_f,

M_2: the small side of the parallelogram joint attached to the foot. Its length is equal to d,

M_3, M_4: the longer sides of the parallelogram joint. Their length is equal to L_b,

M_5: the small side of the parallelogram joint attached to the end-effector,

M_6: the link between M_5 and the end-effector of length e.

Besides these leg elements, there are two other moving masses: the mass of the moving part of the prismatic actuator, M_a, and the one of the end-effector, M_p. The mass of each member M_j is denoted by m_j and the center of mass with respect to the point A_i $(i = 1, 2, 3)$ of each element

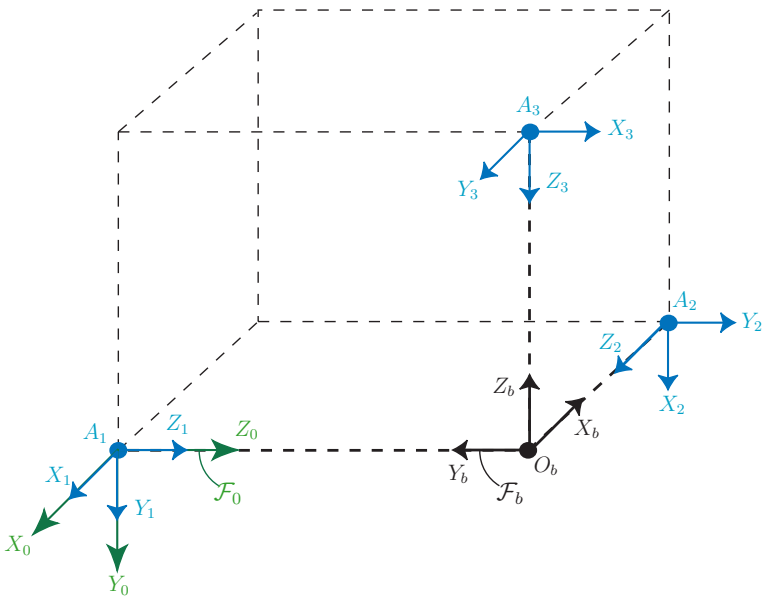

Figure 4: Definition of the reference frames

Table 3: Orthoglide parameters

Parameter	Value	Parameter	Value
m_a	0.300 kg	L_b	0.310 m
m_1	0.248 kg	d	0.080 m
m_2, m_5	0.095 kg	L_f	0.150 m
m_3, m_4	0.117 kg	e	0.031 m
m_6	0.010 kg	λ	45 °
m_p	0.932 kg		

is denoted by C_{ji}, $(j = 1 \dots 6, a, p)$, as shown in Fig. 5. The mass of each element and the geometric parameters of the Orthoglide are presented in Table 3. Assuming that the material of the leg components is homogeneous with center of mass at their geometric center, vectors $\mathbf{c}_{ji}$ of the j^{th} element of the i^{th} leg can be expressed in terms of the geometric $(L_b, L_f, d, e, \lambda)$ and the configuration (q_{1i}, q_{2i}, q_{3i}) parameters of the Orthoglide, as shown in Fig. 5. Therefore, the acceleration $\ddot{\mathbf{c}}_{ji}$ of each element can be calculated. These relations are given in the Appendix. Knowing the mass and acceleration of each element of the i^{th} leg, the shaking forces at the base point of the leg (point A_i) can be calculated by using Eq. (20), i.e.,

$$\mathbf{f}_{sh}^{i} = (m_1 + m_a)\,\ddot{\mathbf{c}}_{1i} + m_2\ddot{\mathbf{c}}_{2i} + m_3\ddot{\mathbf{c}}_{3i} + m_4\ddot{\mathbf{c}}_{4i} + m_5\ddot{\mathbf{c}}_{5i} + m_6\ddot{\mathbf{c}}_{6i} + m_p\ddot{\mathbf{c}}_{pi} \tag{21}$$

The total shaking force at the base frame of the Orthoglide can be obtained by summing up the forces experienced at points A_1, A_2 and A_3. With the definitions of reference frames at points A_i, the total shaking force in the reference frame $\mathcal{F}_0$, of origin point A_1, as shown in Fig. 4, can be written as:

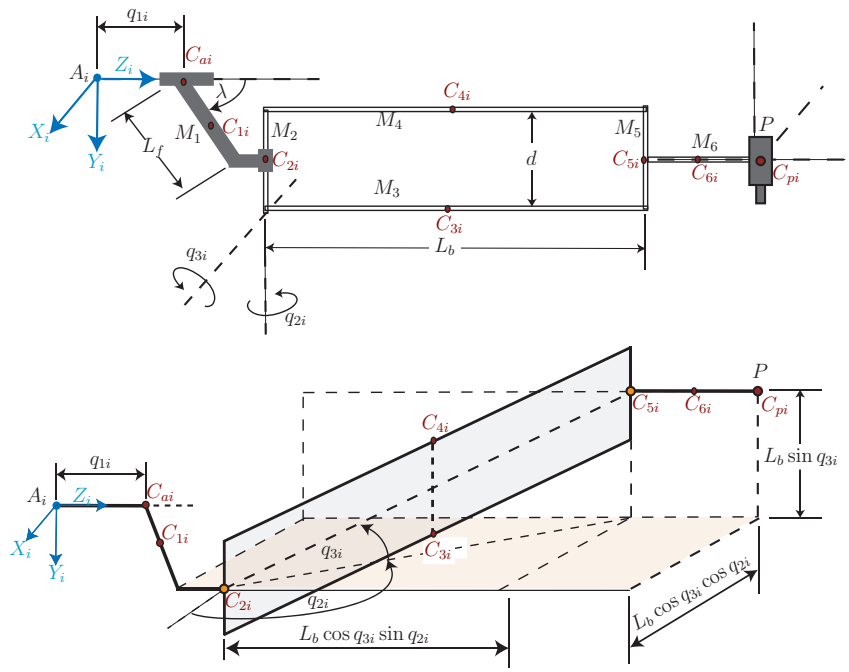

Figure 5: Orthoglide i^{th} leg

$$\mathbf{f}_{sh}^{0} = \begin{bmatrix} F_x^1 + F_z^2 + F_y^3 \\ F_y^1 + F_x^2 + F_z^3 \\ F_z^1 + F_y^2 + F_x^3 \end{bmatrix} \tag{22}$$

The magnitude of the shaking force experienced by the i^{th} actuator at point A_i, can be written as:

$$F_{sh}^{i} = \sqrt{(F_x^i)^2 + \left(F_y^i\right)^2 + (F_z^i)^2} \tag{23}$$

Accordingly, two shaking force indices, defined in Sec. 2.2.2, can be calculated for the given discrete time steps.

3.2.3 Maximum Torque for the Orthoglide

The magnitude of the maximum torque τ_{max} experienced by the Orthoglide actuators can be written as:

$$\tau_{max} = \max\left(\tau_{1_{max}},\ \tau_{2_{max}},\ \tau_{3_{max}}\right) \tag{24}$$

with $\tau_{i_{max}} = \max(\tau_i)$, τ_i being the $1 \times N_t$ dimensional vector of the i^{th} actuator for N_t trajectory points. The inverse dynamic model of the Orthoglide described in [27, 26] is used to evaluate the actuators torques.

3.3 Trajectory Planning and External Forces

In order to apply the methodology proposed for path placement optimization, a rectangular test path is proposed. The test path is defined by the length L and the width W of the rectangle, as shown in Fig. 6(a). Path reference frame $\mathcal{F}_p$ is located at the geometric center of the rectangle. This type of path can be the example of the generation of a rectangular pocket like that of Fig. 6(b). The position of $\mathcal{F}_p$ in the base frame $\mathcal{F}_b$ is defined with the Cartesian coordinates of the origin of $\mathcal{F}_p$, $O_p(x_{O_p},\ y_{O_p},\ z_{O_p})$ and the orientation of $\mathcal{F}_p$ with respect to $\mathcal{F}_b$ is given by Euler's angles, as depicted in Fig. 1(b). For the sake of simplicity, only one of the three rotation angles is considered i.e, rotation about Z_b-axis while X_bY_b and X_pY_p planes

are considered to be always parallel. Accordingly, there are four path placement variables, i.e., $\mathbf{x} = [x_{O_p} \quad y_{O_p} \quad z_{O_p} \quad \phi]^T$, as illustrated in Fig. 6(a).

The magnitude of the end-effector velocity is supposed to be constant along the path. Hence,

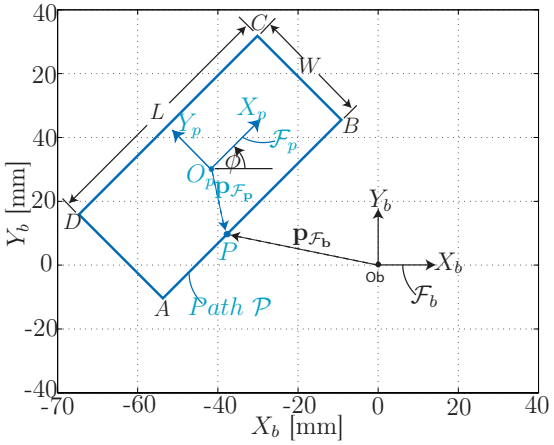

(a) Rectangular test path

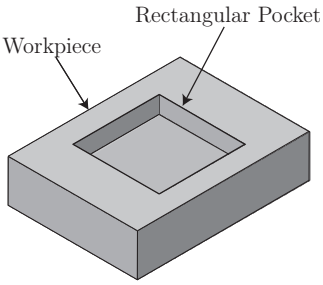

(b) Rectangular pocket

Figure 6: Test path characterization

for given path dimensions, position vector $\mathbf{p}_{\mathcal{F}_\mathbf{p}} = [x_{Pp} \quad y_{Pp} \quad z_{Pp}]^T$ and velocity vector $\mathbf{v}_{\mathcal{F}_\mathbf{p}} = [\dot{x}_{Pp} \quad \dot{y}_{Pp} \quad \dot{z}_{Pp}]^T$ in the path frame can be evaluated as a function of time. Figure 7 shows the position and velocity profiles in $\mathcal{F}_p$ for a 0.05 m×0.10 m rectangular path and for a constant end-effector velocity of 1.0 m.s^{-1}. Position and velocity vectors defined in $\mathcal{F}_p$ can be expressed in $\mathcal{F}_b$ by means of the transformation matrix defined in Eq. (2), namely,

$$\begin{bmatrix} x_{P_b} \\ y_{P_b} \\ z_{P_b} \\ 1 \end{bmatrix} = \begin{bmatrix} C\phi & -S\phi & 0 & x_{Op} \\ S\phi & C\phi & 0 & y_{Op} \\ 0 & 0 & 1 & z_{Op} \\ 0 & 0 & 0 & 1 \end{bmatrix} \begin{bmatrix} x_{P_p} \\ y_{P_p} \\ z_{P_p} \\ 1 \end{bmatrix} \quad , \quad \begin{bmatrix} \dot{x}_{P_b} \\ \dot{y}_{P_b} \\ \dot{z}_{P_b} \\ 1 \end{bmatrix} = \begin{bmatrix} C\phi & -S\phi & 0 & 0 \\ S\phi & C\phi & 0 & 0 \\ 0 & 0 & 1 & 0 \\ 0 & 0 & 0 & 1 \end{bmatrix} \begin{bmatrix} \dot{x}_{P_p} \\ \dot{y}_{P_p} \\ \dot{z}_{P_p} \\ 1 \end{bmatrix}$$

where C and S respectively stands for *cosine* and *sine* functions. For the matter of simplicity and not to deal with tangent and curvature discontinuities, the path is considered to be composed of four independent line segments. Therefore the discontinuities between the segments are neglected.

In order to analyze the effect of external cutting/machining forces in the generation of a given

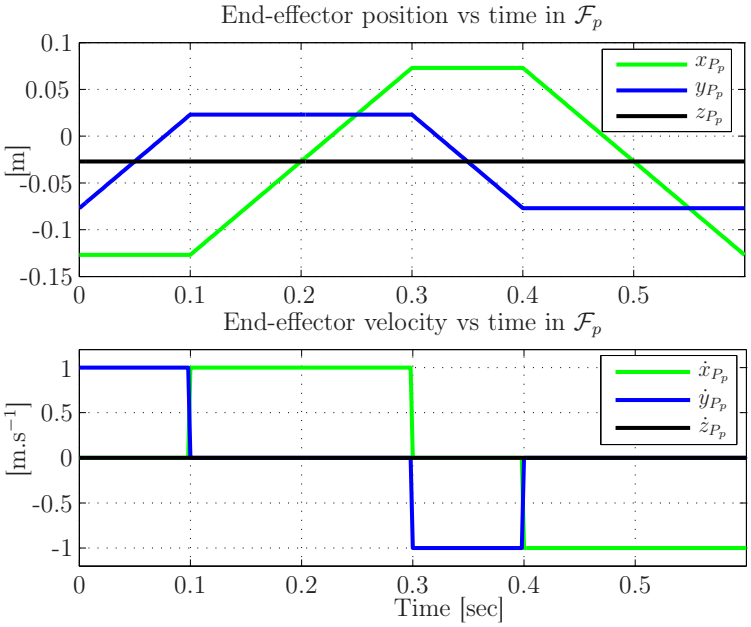

Figure 7: Test trajectory for a rectangular path of size $0.05 \times 0.10\,\mathrm{m}$

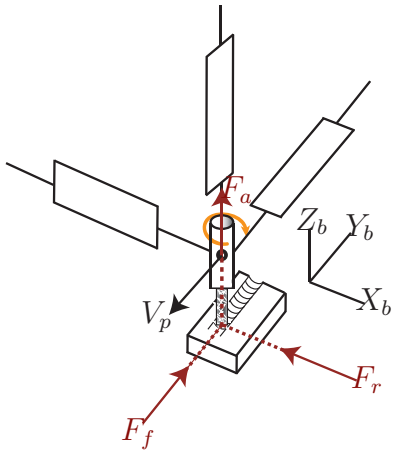

Figure 8: Cutting forces

path, a groove milling operation is considered as shown in Fig. 8 [28]. With constant feed rate or end-effector velocity v_p of magnitude $0.66\,\mathrm{m.s^{-1}}$, i.e, $40\,\mathrm{m.min^{-1}}$, the three components of cutting forces are considered, i.e., component in the feed direction, F_f= 10 N; component along the axis of cutting tool, F_a=25 N; and the component F_r= 215 N, orthogonal to F_f and F_a.

3.4 Results and Discussions

Multiobjective optimum path placement problems are solved for the Orthoglide for the test path described in the previous section. The constraints of the optimization problem are the geometric, kinematic and dynamic ones. The geometric constraints are the upper and lower bounds of the prismatic joints variables. The kinematic constraints are the maximum velocities that the prismatic actuators can produce whereas the dynamic constraints are the limits on the actuators torques. Kinematic and dynamic constraints are specified by the actuators designer and are obtained from the catalogue. As already mentioned, the optimization variables are the coordinates of the origin of path reference frame $\mathcal{F}_p$ and the orientation angle of $\mathcal{F}_p$ with respect to $\mathcal{F}_b$. The numerical values of the constraints used for the Orthoglide are given in Table 2. Multi-objective path placement optimization problem for the Orthoglide can be expressed as,

$$\min_{\mathbf{x}} \left(f_1 : E_t,\ f_2 : I_{\delta f},\ f_3 : I_f,\ f_4 : \tau_{max}\right) \qquad \text{subject to:} \begin{cases} \rho_{min} \leq \rho_{x,y,z} \leq \rho_{max} \\ v_{x,y,z} \leq v_{max} \\ \tau_{x,y,z} \leq \tau_{max} \end{cases} \tag{25}$$

where $\mathbf{x} = [x_{Op} \quad y_{Op} \quad z_{Op} \quad \phi]^T$. The subscripts x, y and z are used for three prismatic actuators or three Cartesian directions.

The problem is modeled with *MATLAB* and *modeFRONTIER* [29]. A multiobjective ge-

Table 4: *modeFRONTIER* algorithm parameters

Scheduler	MOGA-II
Number of iterations	100
Directional cross-over probability	0.5
Selection probability	0.05
Mutation probability	0.1
DNA string mutation ratio	0.05
DOE algorithm	Sobol
DOE number of designs	40
Total number of iterations	$40 \times 100 = 4000$

netic algorithm (MOGA) is used to obtain the Pareto frontiers for a rectangular test path of

dimensions 30 mm×60 mm with an end-effector velocity V_p=0.66 m.s^{-1}. A screen-shot of the *modeFRONTIER* model is shown in Fig. 9 and its scheduler and DOE (design of experiments) parameters are given in Table 4.

The Pareto frontiers obtained are shown in Fig. 10 whereas maximum and minimum (opti-

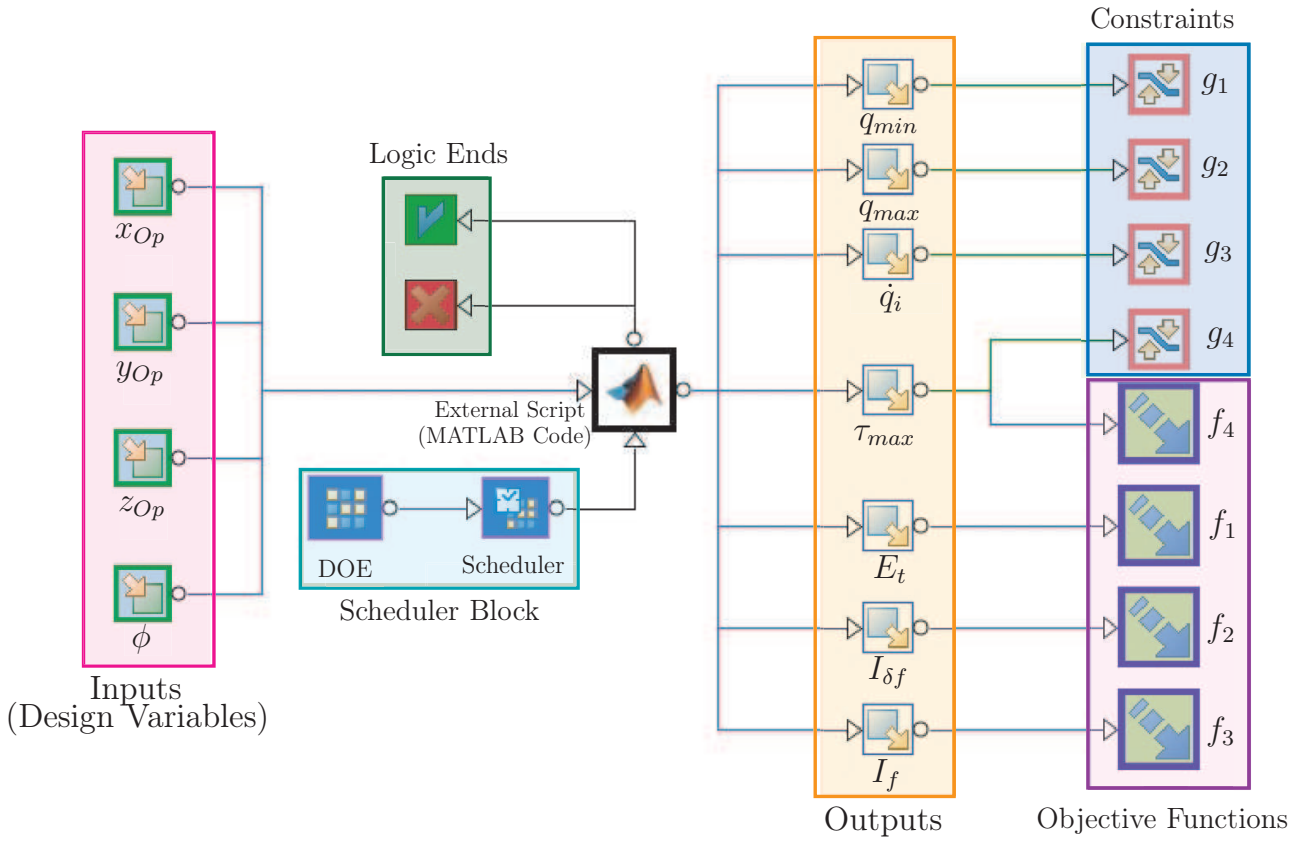

Figure 9: modeFRONTIER model

Table 5: Design parameters that correspond to the Pareto solutions for which the objective functions are either a minimum or a maximum

Objective		x_p [m]	y_p [m]	z_p [m]	ϕ [deg]	Value	Δ	%Δ
E_t [J]	E_{max}	−0.0276	−0.0348	−0.0789	37.2	56.49	33.54	59.38
	E_{min}	0.0141	−0.0044	0.0097	1.44	22.94		
$I_{\delta f}$ [N]	$I_{\delta fmax}$	−0.0204	−0.0693	−0.0019	0.63	2.445	2.41	98.60
	$I_{\delta fmin}$	0.0009	−0.0011	−0.0164	45.0	0.034		
I_f [N]	I_{fmax}	0.0389	−0.0801	−0.1114	40.1	2.620	0.456	17.39
	I_{fmin}	0.0009	−0.0011	−0.0164	45.0	2.164		
τ_{max} [Nm]	τ_{max}	0.0381	−0.0056	0.0714	24.0	1.135	0.287	25.24
	τ_{min}	0.0053	0.0069	−0.1166	42.0	0.849		

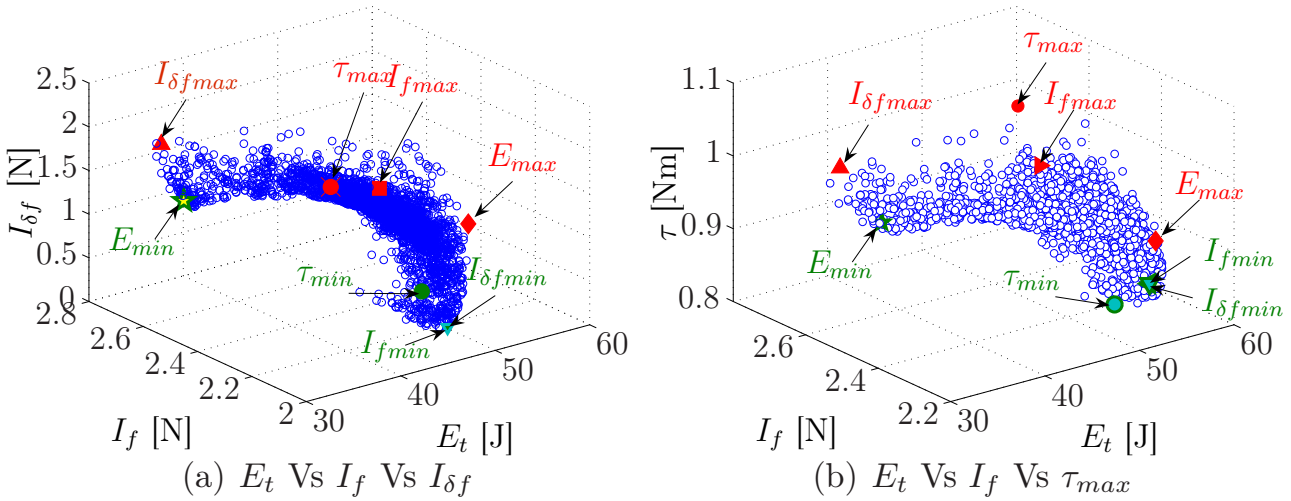

(a) E_t Vs I_f Vs $I_{\delta f}$ (b) E_t Vs I_f Vs τ_{max}

Figure 10: Pareto frontier for the Orthoglide path placement problem

mum) values of each objective, corresponding design parameters and percentage variation (%Δ) are given in Table 5. Path locations in the Orthoglide workspace for maximum and minimum objective functions are shown in Fig. 11.

Table 5 shows that the variations in the shaking forces ($I_{\delta f}$) can be significantly reduced (almost to zero) with an appropriate path placement. As a matter of fact, up to 60% of the energy consumption can be saved with a proper path placement. Maximum shaking forces I_f and maximum actutators torque τ_{max} can be reduced to 17% and 25%, respectively.

Figure 12 shows the shaking forces experienced by the three prismatic actuators of Orthoglide for minimum energy consumption and minimum $I_{\delta f}$ path locations. It can be seen that although the maximum values of the shaking forces for both Pareto-points are almost the same, their variations can be reduced considerably with proper path location. The smoother the shaking force variations, the lower the vibrations in the mechanism. From Table 5 and Fig. 11(a) it can be noted that optimum points with respect to E_t, $I_{\delta f}$ and I_f lie in the neighbourhood of the isotropic configuration of the Orthoglide ($x_p = y_p = z_p \approx 0$) whereas for τ_{max}, z_p attain their minimum value, i.e., at the base of the workspace. Similarly with respect to orientation, ϕ, E_t is minimum for $\phi \approx 0\,^\circ$ and the other three objectives are minimum for $\phi \approx 45\,^\circ$.

Figure 13 summarizes the variational trends as well as the inter-dependency between the objective functions and design variables by means of a scatter matrix. The lower triangular part of

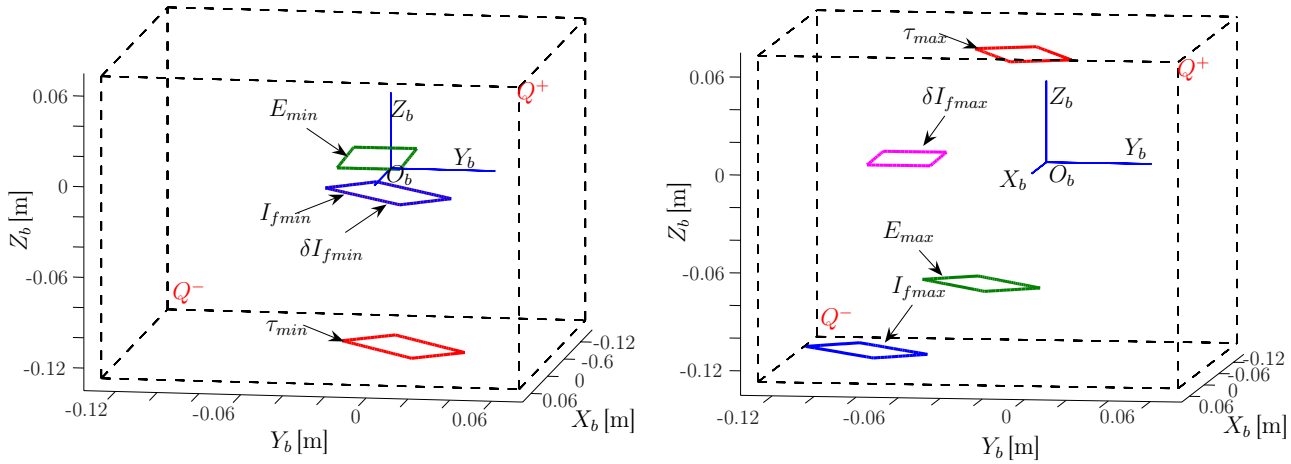

(a) Minimum objectives locations (b) Maximum objectives locations

Figure 11: Path locations in the Orthoglide workspace for minimum and maximum objective functions

the matrix represents the correlation coefficients whereas the upper one shows the corresponding scatter plots. Diagonal elements represents the probability density charts of each variable. The correlation coefficients vary from -1 to 1. Two variables are strongly dependent when their correlation coefficient is close to -1 or 1 and independent when the latter is null. From Fig. 13,

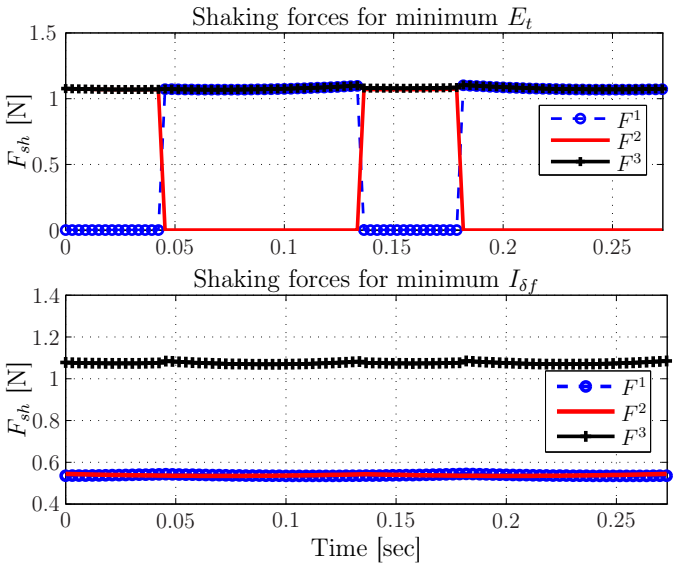

Figure 12: Shaking forces experienced by three actuators for E_{min} and $I_{\delta fmin}$

- E_t, $I_{\delta f}$ and τ_{max} strongly dependent as the correlation coefficients between E_t, $I_{\delta f}$; E_t, τ_{max}; and $I_{\delta f}$, τ_{max} are equal to -0.822, -0.785 and 0.819, respectively. However, the lower

E_t, the higher τ_{max} and $I_{\delta f}$.

- the correlation of I_f with E_t, $I_{\delta f}$ and τ_{max} is very low as the corresponding correlation coefficients are equal to -0.113, 0.185 and -0.065, respectively.
- ϕ has strong and direct correlation with E_t (0.907) whereas it has strong and inverse correlation with $I_{\delta f}$ and τ_{max} (-0.966, -0.828, respectively);
- x_p, y_p, z_p have very week or unpredictable relations with respect to all objectives and parameters.

As $I_{\delta f}$ and τ_{max} are linearly related, the lower $I_{\delta f}$, the lower τ_{max}, no matter the scale of variation of both functions. E_t and τ_{max} are antagonistic. Likewise, E_t and $I_{\delta f}$ are antagonistic. Regarding the design variables, the path orientation ϕ is the most influential for the considered test path. Finally, the foregoing results are only valid for the Orthoglide and the given test path. However, the methodology illustrated in this section is appropriate for any PKM and test path.

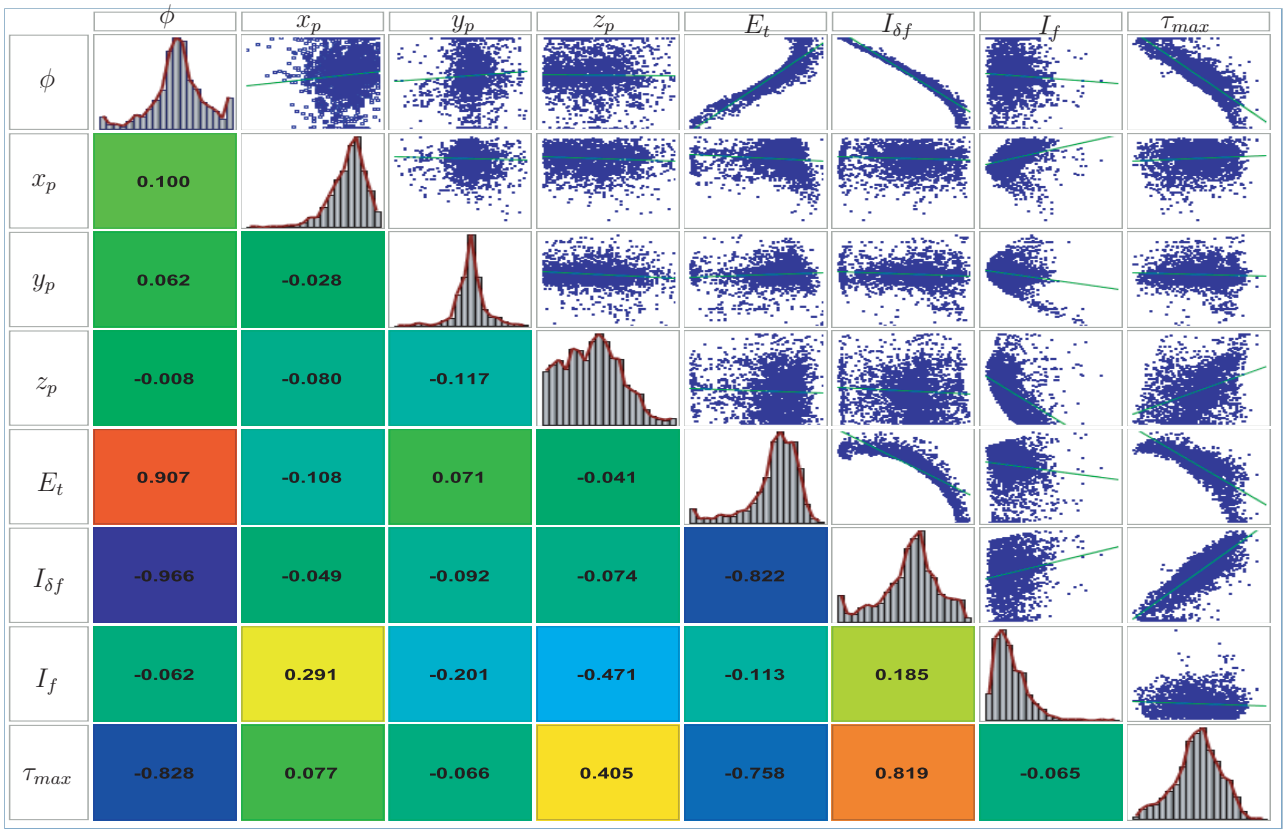

Figure 13: Scatter matrix for objective functions and design variables

4 Conclusions

An approach to optimally locate a given trajectory profile, path or task within the workspace of a PKM is presented. The electric energy consumed by the actuators to carry out that given path is considered as the primary optimization criterion. The electric energy requirement is calculated with the help of the required actuators torques and velocities along with motors electric parameters. Kinematic, velocity and dynamic modeling is used to come up with the trajectory parameters like actuators velocities, accelerations and torques to realize the given path at a certain location in the workspace. To guarantee a realistic solution, actuators performance limits such as their joint limits, maximum velocities and torque capabilities are used as the constraints of the optimization problem. The minimization of the effects of the shaking forces and minimization of the actuators peak torques are considered as other optimum path placement criteria, hence obtaining a multiobjective optimization problem.

The proposed methodology is applied to the Orthoglide, a 3-DOF translating PKM with a regular cubic workspace. A rectangular shaped test path is considered as an illustrative example. Such a path can be used to realize pocketing operations.

The use of the electric energy instead of the mechanical energy as an optimization criterion is pertinent. Although actuator electric energy consumption depends on the mechanical energy requirements, the electric energy evaluation is more comprehensive than its mechanical counterpart. The general approach used to calculate the mechanical energy with the help of velocity and dynamic models, i.e., by using actuators torques and velocities, may lead to an under estimation of the energy requirements in the case where actuators are experiencing torques with zero velocities. Besides, usual mechanical energy calculations do not consider the resistive energy loss in the motors windings as well as the energy loss due to the variations in the actuators velocities. Those variations affect the current requirements and hence induce electromotive forces in the actuators. Accordingly, the electric energy formulation takes into account all these energy losses.

The energy required to perform a given task depends on the position and the orientation of the

task within the workspace. Accordingly, some electric energy can be saved by properly selecting the position and the orientation of the task. Indeed, a misplaced task can cause excessive energy consumption and can force the actuators to go over their performance limits. For the Orthoglide, the optimum path location is found to be in the neighbourhood of the isotropic configuration but there is no general rule to predict the exact optimal position and orientation of a task particularly for a complicated three dimensional task or for an irregular workspace. However, a detailed analysis of the energy variation within the workspace for a given task can lead to the optimal position/orientation of that particular task. Numerical optimization algorithms are useful for such a comprehensive analysis in which all the problem constraints and performance measures can be considered simultaneously.

Variations in the shaking forces experienced by the base platform of a PKM also vary with the path location. However, the lower the shaking forces, the higher the energy consumption. The magnitude of the maximum shaking forces can also be reduced with path location but to a lower extent compared to the reduction of the variations in the shaking forces. Similarly, the magnitude of the maximum actuators torques can be reduced with appropriate path location. However, the energy consumption would increase with the minimization of the shaking forces effects and maximum torques. Hence, a trade-off has to be made by the user.

In the future work, some multi-objective problems will be treated with more objectives and constraints and with complex tasks and irregular workspaces. Furthermore, along with shaking forces, shaking moments will also be considered.

Acknowledgements

The support of the Higher Education Commission (HEC) Pakistan, under HEC overseas scholarship program, held by the first author, is dutifully acknowledged.

References

[1] A. A. Ata, "Optimal trajectory planning of manipulators: A review," *Journal of Engineering Science and Technology*, Vol. 2 (1), pp. 32–54, 2007.

[2] L. Tian and C. Collins, "Motion planning for redundant manipulators using a floating point genetic algorithm," *Journal of Intelligent and Robotic Systems, Theory and Applications*, Vol. 38(3-4), pp. 297–312, 2003.

[3] K. K. Chan and A.M.S. Zalzala, "Genetic-based minimum time trajectory planning of articulated manipulators with torque constraints," *IEEE Colloquium on Genetic Algorithms for Control Systems Engineering*, London, 4/1–4/3, 1993.

[4] V. Pateloup, E. Duc and P. Ray, "Corner Optimization for pocket machining," *International Journal of Machine Tools and Manufacture*, Vol. 44(12–13), pp. 1343–1353, 2004.

[5] G. Field, "Iterative dynamic programming, an approach to minimum energy trajectory planning for robotic manipulators," *Proc. of the IEEE Int. Conf. on Robotics and Automation*, Minneapolis, Vol. 3, pp. 2755–2760, 1995.

[6] A. Hirakawa and A. Kawamura, "Trajectory planning of redundant manipulators for minimum energy consumption without matrix inversion," *Proc. of the IEEE Int. Conf. on Robotics and Automation*, New Mexico, pp. 2415–2420, 1997.

[7] B. Nelson and M. Donath, "Optimizing the location of assembly tasks in a manipulators workspace," *Journal of Robotic System*, Vol. 7(6) pp. 791–811, 1990.

[8] N. A. Aspragathos, "Optimal location of path following tasks in the workspace of a manipulator using genetic algorithm," *ARK'96, Published in Recent Advances in Robot Kinematics*, Kluwer Academic Publishers, Portroz, Slovinia, pp. 179–188, 1996.

[9] N. A. Aspragathos and S. Foussias, "Optimal location of a robot path when considering velocity performance," *Robotica*, Vol. 20, pp. 139–147, 2002.

[10] B. Fardanesh and J. Rastegar, "Minimum cycle time location of a task in the workspace of a robot arm," *Proc. of the 27th Conf. on Decision Control*, Austin, Texas, pp. 2280–2283, 1988.

[11] J. T. Feddema, "Kinematically optimal robot placement for minimum time coordinated motion," *Proc. of the IEEE 13th Int. Conf. on Robotics and Automation*, Part 4, pp. 22–28, 1996.

[12] J. S. Hemmerle and F.B. Prinz, "Optimal path placement for kinematically redundant manipulators," *Proc. of the IEEE Int. Conf. on Robotics and Automation*, Vol. 2, pp. 1234–1244, 1991.

[13] G.J.A. Pamanes and S. Zeghloul, "Optimal placement of robotic manipulators using multiple kinematic criteria," *Proc. of the 1991 IEEE Int. Conf. on Robotics and Automation*, Vol. 1, pp. 933–938, 1991.

[14] G.J.A. Pamanes, S. Zeghloul, and J. Lallemand, "On the optimal placement and task compatibility of manipulators," *Proc. of the IEEE Int. Conf. on Advanced Robotics-'91 ICAR*, Vol. 2, pp. 1694–1697, 1991.

[15] G.J.A. Pamanes, E. Cuan-Duron, and S. Zeghloul, "Single and multiobjective optimization of path placement for redundant robotic manipulators," *Ingeniería Investigación y Tecnología*, Vol. 9(3), pp. 211-237, 2008.

[16] Z. Wang, C. Wang, W. Liu and Y. Lei, "A study on workspace, boundary workspace analysis and workpiece positioning for parallel machine tools," *Mechanism and Machine Theory*, Vol. 36(5), pp. 605–622, 2001.

[17] R. Ur-Rehman, S. Caro, D. Chablat and P. Wenger, "Path placement optimization of manipulators based on energy consumption: application to the orthoglide 3-axis," *Transactions of the Canadian Society for Mechanical Engineering*, http://arxiv.org/abs/0910.4000, to appear, 2009.

[18] G. Lacroux, "Les actionneurs lectriques pour la robotique et les asservissements," Technique et Documentation Lavoisier, 2nd edition,Paris, 1994.

[19] S.T. Chiou, G.J. Bai and W.K. Chang, "Optimum balancing design of the drag-link drive of mechanical presses for precision cutting," *International Journal of Machine Tools and Manufacture*, Vol. 38(3), pp. 131–141, 1998.

[20] Y. Wu and C.M. Gosselin, "Synthesis of reactionless spatial 3-dof and 6-dof mechanisms without separate counter-rotations," *The International Journal of Robotics Research*, Vol 23 (6), pp. 625–642, 2004.

[21] B. Moore, J. Schicho and C. M. Gosselin, "Determination of the complete set of shaking force and shaking moment balanced planar four-bar linkages," Mechanism and Machine Theory, In Press, Corrected Proof, Available online 9 December 2008.

[22] R. Clavel, "Delta, a fast robot with parallel geometry," *Proc. of 18th Int. Symposium on Industrial Robots*, pp. 91–100, April 1988.

[23] P. Wenger and D. Chablat, "Kinematic analysis of a new parallel machine tool: The Orthoglide," in: Lenarcic, J. and Stanisic, M.M. (editors), Advances in Robot Kinematic, Kluwer Academic Publishers, pp. 305–314, 2000.

[24] A. Pashkevich, D. Chablat, and P. Wenger, "Stiffness analysis of overconstrained parallel manipulators," *Mechanism and Machine Theory*, Vol. 44(5), pp. 966–982, May 2009.

[25] D. Chablat and P. Wenger, "Architecture Optimization, of a 3-DOF Parallel Mechanism for Machining Applications, The Orthoglide," *IEEE Transactions on Robotics and Automation*, Vol. 19, pp. 403–410, 2003.

[26] S. Guégan, W. Khalil et Ph. Lemoine, "Identification of the Dynamic Parameters of the Orthoglide," *IEEE Int. Conf. on Robotics and Automation*, Taipei, Taiwan, Vol. 3, pp. 3272–3277, 14–19 Sept. 2003.

[27] S. Guegan and W. Khalil, "Dynamic modeling of the Orthoglide," Advances in Robot Kinematic, Kluwer Academic Publishers, Caldes de Malavella, Spain, pp. 387–396, 2002.

[28] F. Majou, C. Gosselin, P. Wenger and D. Chablat, "Parametric stiffness analysis of the Orthoglide," *Mechanism and Machine Theory*, Vol. 42(3), pp. 296 – 311, March 2007.

[29] modeFRONTIER, Version 4.0.3, ESTECO, Trieste, Italy, URL http://www.esteco.it.

Appendix

Expressions of $\mathbf{c}_{ji}$, $j = 1 \dots 6,\ a,\ p$ and $i = 1, \dots, 3$, used for the calculations of the shaking forces for the Orthoglide with reference to Fig. 5, (C and S respectively stand for *sine* and *cosine* functions):

$$\mathbf{c}_{ai} = [0 \quad 0 \quad q_{1i}]^T \tag{A.1}$$

$$\mathbf{c}_{1i} = \left[0 \quad \frac{L_f}{2}S\lambda \quad q_{1i} + \frac{L_f}{2}C\lambda\right]^T \tag{A.2}$$

$$\mathbf{c}_{2i} = [0 \quad L_f S\lambda \quad q_{1i} + L_f C\lambda]^T \tag{A.3}$$

$$\mathbf{c}_{3i} = \left[\frac{L_b}{2}Cq_{3i}Cq_{2i} \quad L_f S\lambda + \frac{d}{2} - \frac{L_b}{2}Sq_{3i} \quad q_{1i} + L_f C\lambda + \frac{L_b}{2}Cq_{3i}Sq_{2i}\right]^T \tag{A.4}$$

$$\mathbf{c}_{4i} = \mathbf{c}_{3i} + [0 \quad d \quad 0]^T \tag{A.5}$$

$$\mathbf{c}_{5i} = [L_b Cq_{3i}Cq_{2i} \quad L_f S\lambda - L_b Sq_{3i} \quad q_{1i} + L_f C\lambda + L_b Cq_{3i}Sq_{2i}]^T \tag{A.6}$$

$$\mathbf{c}_{6i} = \mathbf{c}_{5i} + [0 \quad 0 \quad e/2]^T \tag{A.7}$$

$$\mathbf{c}_{pi} = \mathbf{c}_{5i} + [0 \quad 0 \quad e]^T \tag{A.8}$$

Twice differentiating Eqs. A.1 to A.8, result:

$$\ddot{\mathbf{c}}_{ai} = [0 \quad 0 \quad \ddot{q}_{1i}]^T \tag{A.9}$$

$$\ddot{\mathbf{c}}_{1i} = \ddot{\mathbf{c}}_{ai} \tag{A.10}$$

$$\ddot{\mathbf{c}}_{2i} = \ddot{\mathbf{c}}_{ai} \tag{A.11}$$

$$\ddot{\mathbf{c}}_{3i} = \begin{bmatrix} \frac{L_b}{2}(-\dot{q}_{2i}^2 Cq_{3i}Cq_{2i} - \ddot{q}_{2i}Cq_{3i}Sq_{2i} + 2\dot{q}_{2i}\dot{q}_{3i}Sq_{2i}Sq_{3i} - \dot{q}_{3i}^2 Cq_{2i}Cq_{3i} - \ddot{q}_{3i}Cq_{2i}Sq_{3i}) \\ \frac{L_b}{2}\left(\dot{q}_{3i}^2 Sq_{3i} - \ddot{q}_{3i}Cq_{3i}\right) \\ \ddot{q}_{1i} + \frac{L_b}{2}(-\dot{q}_{3i}^2 Cq_{3i}Sq_{2i} - \ddot{q}_{3i}Sq_{3i}Sq_{2i} - 2\dot{q}_{2i}\dot{q}_{3i}Sq_{3i}Cq_{2i} - \dot{q}_{2i}^2 Cq_{3i}Sq_{2i} + \ddot{q}_{2i}Cq_{3i}Cq_{2i}) \end{bmatrix} \tag{A.12}$$

$$\ddot{\mathbf{c}}_{4i} = \ddot{\mathbf{c}}_{3i} \tag{A.13}$$

$$\ddot{\mathbf{c}}_{5i} = \begin{bmatrix} L_b(-\dot{q}_{2i}^2 Cq_{3i}Cq_{2i} - \ddot{q}_{2i}Cq_{3i}Sq_{2i} + 2\dot{q}_{2i}\dot{q}_{3i}Sq_{2i}Sq_{3i} - \dot{q}_{3i}^2 Cq_{2i}Cq_{3i} - \ddot{q}_{3i}Cq_{2i}Sq_{3i}) \\ L_b\left(\dot{q}_{3i}^2 Sq_{3i} - \ddot{q}_{3i}Cq_{3i}\right) \\ \ddot{q}_{1i} + L_b(-\dot{q}_{3i}^2 Cq_{3i}Sq_{2i} - \ddot{q}_{3i}Sq_{3i}Sq_{2i} - 2\dot{q}_{2i}\dot{q}_{3i}Sq_{3i}Cq_{2i} - \dot{q}_{2i}^2 Cq_{3i}Sq_{2i} + \ddot{q}_{2i}Cq_{3i}Cq_{2i}) \end{bmatrix} \tag{A.14}$$

$$\ddot{\mathbf{c}}_{6i} = \ddot{\mathbf{c}}_{5i} \tag{A.15}$$

$$\ddot{\mathbf{c}}_{pi} = \ddot{\mathbf{c}}_{5i} \tag{A.16}$$